PAPER

Reinventing the wheel: excitation of flow instabilities for active flow control using plasma actuators

View the article online for updates and enhancements.

IOP ebooks™

Bringing you innovative digital publishing with leading voices to create your essential collection of books in STEM research.

Start exploring the collection - download the first chapter of every title for free.

Reinventing the wheel: excitation of flow instabilities for active flow control using plasma actuators

Mo Samimy[iD], Nathan Webb and Ata Esfahani[iD]

Gas Dynamics and Turbulence Laboratory, Aerospace Research Center, The Ohio State University,
Columbus, OH 43235, United States of America

E-mail: Samimy.1@osu.edu

CrossMark

Abstract

Flow control is typically used to manipulate a flow's natural behavior to alter its effects on
a vehicle or system. When active flow control (AFC) is used in aerospace applications, the
actuation can be turned on/off or adapted to changing flight conditions. AFC techniques in
which significant gains can be achieved with relatively small cost are most beneficial and
are the subject of this paper. Flows with the Kelvin–Helmholtz (K–H) instability, which are
present in many aerospace applications, are amenable to AFC and have been the subject of
research for over five decades. The K–H instability can amplify any natural or artificially-
seeded thermal, acoustic, or hydrodynamic perturbations over a wide range of frequencies.
These perturbations can grow and eventually roll up into large-scale flow structures, which,
in turn, can dominate important processes such as entrainment, mixing, momentum and heat
trasport, and aeroacoustic noise. However, the application of active flow control was limited
to low-speed flows in the earlier decades of study due to the shortcomings of the available
actuators. The recent development of plasma actuators, capable of producing simultaneously
high-amplitude and high-bandwidth thermal perturbations, has extended the AFC applications
to high-speed and high-Reynolds number flows of interest in aerospace, hence the title:
reinventing the wheel. In this paper, two classes of such plasma actuators, namely localized
arc filament plasma actuators and nanosecond dielectric-barrier discharge plasma actuators,
are briefly discussed and their applications in two very different flows are presented to
highlight the advances made in the community in the use of plasma actuators for aerospace
applications. In addition, there is a discussion of further advances that must be made in the
development of these actuators to move the techniques from laboratory to in-flight use.

Keywords: plasma actuators, thermal perturbations, active flow control,
excitation of Kelvin–Helmholtz instability

(Some figures may appear in colour only in the online journal)

1. Introduction

Fluid flows are ubiquitous in nature and in engineered sys-
tems. Nearly all aerospace applications entail high speed and
high Reynolds number (thus turbulent) flows. Such flows
contain structures over a wide range of scales, their behavior
is quite complex to understand, and the governing equa-
tions are nonlinear and difficult to solve. Over many decades,
tremendous effort has gone into developing experimental,
computational, and controls tools and capabilities to gain a
better understanding of their physics, to more accurately pre-
dict their behavior, and to more effectively control them. The
simplest flow control techniques involve geometrical modifi-
cations, e.g. vortex generators on aircraft wings for flow sepa-
ration control or chevrons at the exhaust nozzle of a jet aircraft
to reduce community noise at takeoff and landing. While these

passive devices work as intended at the design flight conditions, they often have detrimental effects during the other portions of the flight.

Active flow control (AFC), on the other hand, can be engaged only when required and the actuation can be adapted to the flight conditions. This ability makes it more desirable than its passive counterpart; however it does require initial installation and recurring maintenance and operational cost. Therefore, the benefits gained by the use of AFC must outweigh the cost in order for its use to be practical. Assuming the initial installation and maintenance costs are acceptable, the operational cost must be minimal to make an AFC technique more attractive than a passive technique. AFC techniques in which significant gains can be achieved with relatively small cost are most desirable. Flows with the Kelvin–Helmholtz (K–H) instability, which are present in many aerospace applications, are amenable to such control and have been the subject of research for over five decades. Early observations [1] that the flame of a gas burner was swaying to the beats of classical music appear to be the first step in recognizing the instability in free-shear flows. Such flows where a shear layer develops away from any solid surface, exist in many practical aerospace applications including jets, cavity flows, and separated flows of various kind from vehicle surfaces.

Two seminal discoveries in free-shear flows occurred in the 1960s and 70s. The first was finding, through theoretical analyses, that free shear flows are amenable to excitation by small perturbations over a wide range of frequencies [2–4]. This instability is called the Kelvin–Helmholtz instability, which is an essentially inviscid (i.e. with negligible viscous effect) mechanism in high-speed and high Reynolds number flows of aerospace applications. The second discovery was the existence of coherent large-scale flow structures in free shear flows in experimental work, even at relatively high Reynolds numbers, and the connection between these structures and the K–H instability [5, 6]. The dynamics of these structures are known to dominate important processes such as entrainment, mixing, momentum and heat transport, and noise generation in turbulent flows. Crow and Champagne [5] showed that axisymmetric free-shear flows or jets can act as a band-pass amplifier of perturbations in the flow and generate and support coherent large-scale flow structures. Brown and Roshko [6] serendipitously discovered the existence of coherent large-scale structures in high Reynolds number planar free shear-flows while investigating the effect of flow density on mixing layers.

Tremendous progress was made in the 1970s and 80s in the use of AFC to excite flow instabilities by providing acoustic or hydrodynamic perturbations. However, the early experimental research focused almost exclusively on low-speed, low Reynolds number flows (e.g. $Re_D < 50\,000$ in jets). As the flow speed and Reynolds number increase, so do the turbulence level and instability frequencies, requiring high-amplitude, high-bandwidth perturbations to excite the instabilities. These two opposing requirements were largely beyond the capabilities of the mechanical, fluidic, and acoustic actuators that were used in the early works. As a result, there were practically no experimental works in the active control of high-speed

and high Reynolds number free-shear flows. Among the few exceptions is, for example, Kibens *et al*'s work [7], which successfully used high amplitude pulsed fluidic injection to excite flow instability in the jet exhaust from a full-scale JT8D jet engine (used in heavy lift military transport). The significant increase in the scale (with the commensurate decrease in the required excitation frequency) made this work possible, but it clearly demonstrated the applicability of instability theory and AFC in high-speed and high Reynolds number free shear flows. It should be noted that the term 'excitation' in this paper is used in the context of excitation of flow instabilities and amplification of the seeded perturbations. Ho and Huerre [8] cover most of the developments on the subject until the mid 1980s and Samimy *et al* [9] those made thereafter.

Plasma actuators have been employed for AFC for over 50 years [10]. Martens *et al* [11] performed a very early work to excite free-shear flow instabilities, demonstrating a significant effect of excitation on the growth rate and spectral content of a developing shear layer in high-speed, low Reynolds number free-shear flow. However, the use of plasma actuators for AFC began in earnest primarily in the early 2000s. Various surface and volume-filling plasmas, including DC, AC, RF, microwave, arc, corona, and spark discharges, have been used to control flows. The primary mechanisms of plasma flow control include electrohydrodynamic (EHD) and magnetohydrodynamic (MHD) interactions, both of which are typically used to impart momentum to the flow, and thermal (Joule) heating. Three classes of plasma actuators have been developed and extensively used for flow control over the past 15 years. The first, and most widely used, are based on EHD and called alternating current dielectric barrier discharge (AC-DBD) plasma actuators [12]. The other two are based on Joule heating: localized arc filament plasma actuators (LAFPA) [9, 13, 14] and nanosecond dielectric barrier discharge (NS-DBD) plasma actuators [15]. These two actuators are very different in nature, but both, especially LAFPAs, can provide high-amplitude and high-bandwidth perturbations for control of free-shear flow instabilities in high-speed, high Reynolds number flows. They have begun filling a void that existed in excitation of instabilities in free-shear flows since 1980s.

The focus of this paper is on the utilization of two well-known classes of plasma actuators for controlling flows with the K–H instability and wide-ranging aerospace applications. Two example problems from this class of flows are presented to highlight some of the advances in AFC using plasma actuators. In what follows, a brief description of these two actuators will be provided along with references for detailed information for the interested reader. That will be followed by a brief overview of the K–H instability intended for the plasma community. Then some results from these two flows will be presented and discussed to show the effectiveness of control.

2. Plasma actuators

Actuator is one of the most important components of any AFC technique. The actuators used in the 1970s and 1980s for excitation of the K–H instability in the flows were primarily acoustic, mechanical, or fluidic. However, as the flow speed
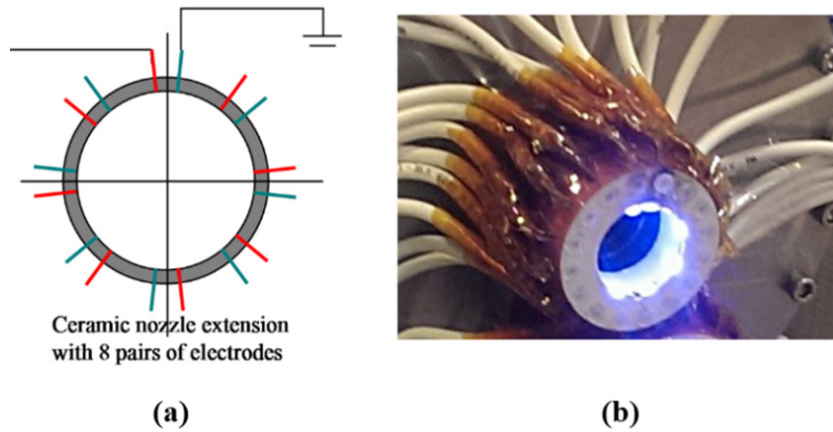
J. Phys. D: Appl. Phys. **52** (2019) 354002

M Samimy *et al*

Figure 1. (a) Schematic of eight LAFPAs distributed near a nozzle exit and (b) a photograph showing the glow from the active actuators near the nozzle exit. From [9]. Reprinted by permission of the American Institute of Aeronautics and Astronautics, Inc.

and Reynolds number increase, so do the frequencies most amplified by the K–H instability and the perturbation amplitude required to excite it. Therefore, the actuators for excitation of instabilities in the high-speed turbulent flows relevant to aerospace applications must generate wide-bandwidth and high-amplitude perturbations. Acoustic actuators can meet the former and mechanical and fluidic actuators can meet the latter requirements, however, neither can simultaneously meet both. Interested readers are referred to a recent review article covering acoustic, mechanical, and fluidic actuators and their application [16]. Until about 15 years ago, when the development of plasma actuators began in earnest, there was a major void in the field of AFC in aerospace applications.

The primary mechanisms of plasma flow control include EHD and MHD interactions and thermal (Joule) heating. EHD and MHD interactions involve flow entrainment by collisional momentum transfer to the fluid from charged species accelerated by Coulomb and Lorentz forces, respectively. For MHD flow control, the primary limitation is sustaining sufficient flow conductivity under high mass flow rate conditions. The main limitation of the use of EHD flow control is generating sufficient ion densities in the cathode sheath (space-charge region) of the discharge. Examining the most commonly used actuators today, it is observed that AC-DBD actuators are based on EHD and NS-DBD actuators and LAFPAs are based on Joule heating. AC-DBD and NS-DBD actuators use an identical actuator geometry. The primary difference is in the input voltage waveform: it is a sinusoidal waveform for the former and a pulsed waveform for the latter. This makes a tremendous difference in the actuator's output: it is induced velocity/momentum for the former and thermal perturbations for the latter [17]. Simple estimates [18] show that a significant EHD effect on the boundary layer flow can be achieved at flow velocities of up to $U_\infty \sim 100$ m s^{-1}. This is consistent with experimental results using AC-DBD actuators on flow separation control over an airfoil, demonstrated at U_∞ up to ~50 m s^{-1} [12]. It has been shown in recent years that by using much higher input voltage to the actuator and a much thicker dielectric barrier, AC-DBD actuators can maintain control authority at flow speeds up to ~135 m s^{-1} [19]. There are comprehensive recent review articles on this class of plasma

actuators [12, 20, 21], therefore, they will not be further discussed in this paper.

In this section, brief descriptions of LAFPAs and NS-DBD actuators, which have been used extensively in aerospace application-oriented research flows in recent years, will be provided. Interested readers are referred to the cited references for more detailed information.

2.1. Localized arc filament plasma actuators (LAFPAs)

Leonov *et al* [22] were first to suggest that significant high-speed flow control could be realized using the thermal effects of near-surface, high-current, high-temperature arc discharges. They showed that intense, localized, rapid heating produced by plasmas in high-current, pulsed, electric discharges have the control authority needed to modify even supersonic flows. LAFPAs—introduced in 2004 [23]—built and expanded upon this concept. LAFPAs were designed to excite flow instabilities in high-speed, high-Reynolds number flows and were specifically developed to address the shortcomings of other types of actuators for this purpose, particularly the difficulty of producing simultaneously wide-bandwidth, high-amplitude perturbations [13, 14]. In this approach, rapid, near-adiabatic heating in the current filament, which also results in compression waves is employed to excite the instabilities in high Reynolds number jets [13, 14]. This topic will be revisited later in this section. A schematic and photograph of these actuators are shown in figure 1. In the earlier work, the electrodes were flush mounted with the inner surface of the nozzle. However, the plasma was noticeably stretched by the high-speed flow and eventually swept downstream, reducing the effectiveness of actuation [23]. Therefore, the electrode tips and plasma arc are now recessed in a circular groove, 0.5 mm deep and 1.0 mm wide, to improve discharge stability and prevent plasma blow-off. This groove (confirmed not to significantly affect control authority [24]), shields the arc filament, allowing it to be sustained and pulsed at any desired frequency to most effectively excite natural flow instabilities over a wide range of frequencies.

There are several variations of pin-electrode-based plasma actuators besides LAFPAs [25–27]. In the first two references,

J. Phys. D: Appl. Phys. **52** (2019) 354002

M Samimy *et al*

the electrodes are located in a small cavity and can be used to generate a pulsed high-speed control jet. In the last example [27], the electrodes are located at the throat of a cavity with converging or converging-diverging walls to perturb the sonic flow at the throat. The actuators in the first two references [25, 26] are high-amplitude actuators and have been successfully used in several flows. However, their bandwidth is limited due to the time required to refresh the fluid in the cavity. Adelgren *et al* [28] used only a single pair of electrodes located at the nozzle exit to control a high-speed jet.

The concept and initial development of LAFPAs are presented in [23]. Later evolution and characterization of LAFPAs, as well as the differences between LAFPAs and other plasma based actuators, are given in [9, 13, 14]. In its basic form, a LAFPA consists of a pair of electrodes, one connected to ground and the other to a pulsed high-voltage (several kV) source (figure 1(a)). In typical laboratory experiments, the actuators are located approximately 1 mm upstream of the shear layer origin and the center-to-center distance between the two electrodes is typically 3–4 mm (figure 1(b)). Right after the flow exits the nozzle, the shear layer is formed and that is where the K–H instability is most receptive to the introduction of perturbations. High-voltage pulses are applied to each actuator by means of an electronically controlled switch. The high initial voltage is required to achieve breakdown in the approximately atmospheric pressure air in the gap between the electrodes. When the voltage across a pair of electrodes reaches the breakdown voltage, the air between the electrodes breaks down and an electric arc is established. After breakdown, the voltage across the electrodes drops to a few hundred volts and remains at that level until the voltage source is disconnected. The frequency and duty cycle/pulse width are controlled independently for each actuator and limits (determined by the power supply) are typically 10s to 100s of kHz, and 1 μs to 1 ms. Past results have demonstrated that complete breakdown of the air is crucial to achieving significant control authority [24, 29].

Moore [30] argued that shear layers are receptive to thermal, acoustic, and hydrodynamic perturbations, provided the perturbations are spanwise/azimuthally coherent. In the jet example case, shown in figure 1, eight LAFPAs are distributed uniformly along the nozzle exit perimeter to provide the most azimuthally (spanwise) uniform perturbations possible. In addition, the eight actuators can be operated with phase delays with respect to one another to excite different azimuthal modes, the significance of which will be discussed later. The actuators are located approximately 1 mm upstream of the nozzle exit, as close to the origin of the shear layer as physically possible, as that is the region of greatest receptivity for excitation of instability [31].

The initial perturbations in LAFPAs as well as in NS-DBDs, discussed in the following section, are thermal, and with flow being compressible, the rapid thermal perturbations lead to the formation of compression waves. As Moore noted [30], either one of these two perturbations or a combination of the two can excite the flow instability. However, recent work [32] suggests that it is primarily the thermal perturbation at work in AFC. This issue will be revisited later. In a high-fidelity

computational work, Gaitonde and Samimy [33] used a simple surface heating model, based on the experimentally measured temperature perturbations, to represent the actuation. This methodology produced mean flow results and large-scale flow structures with various azimuthal modes which compared quite well with experimental results, providing futher evidence of the Joule-heating-nature of these actuators' control mechanism.

As the power supplies are the primary component of the LAFPAs, substantial effort has been invested in improving their design. The three most important aspects of the power supply will be briefly highlighted, but details can be found in [9]. The first is the excitation bandwidth. The rapid changes in the current associated with pulsing the actuators cause significant energy dissipation within the power supply. This energy dissipation scales linearly with frequency. Thus, increasing the available bandwidth typically involves improving heat dissipation. While the frequency-response of the driving electronics controls the minimum rise time of the voltage to breakdown levels, effectively limiting the maximum theoretical frequency of the discharge, in practice insufficient heat dissipation is typically the limiting factor. In a laboratory with small-scale experiments, the required frequency for excitation of instabilities in typical aerospace application-oriented flows is very high. However, in application (i.e. larger scales) the need for high frequency is eased, a fact exploited by the early instability-based AFC work of Kibens *et al* [7]. Second, while some level of electro-magnetic interference (EMI) will always be generated by the arc, the vast majority of EMI is radiated by the power cables and internal power supply circuitry. This problem poses a significant concern for utilization of this technology and must be addressed before it can be implemented in application. However, as it can typically be avoided via adequate shielding in a laboratory environment, little consideration has been given to it in the design of the power supplies in our laboratory. Third, the electronic efficiency of the power supply is lower than desired and must be improved.

The impulsive nature of LAFPA excitation, given that the breakdown provides bulk of the perturbation, results in the introduction of perturbations not only at the fundamental actuation frequency, but also at several super-harmonics. This is readily seen in near-field pressure-fluctuation spectra (figure 2) collected from an excited Mach 0.9 jet [34]. For these measurements, a microphone is located just outside the jet so it can detect the passage of large-scale flow structures formed in the shear layer of the jet due to the K–H instability. The high-amplitude nature of the LAFPA-produced perturbations ensures that at least one of the several super-harmonics has sufficient amplitude to excite the natural flow instabilities, which will be further discussed later. In figure 2, the actuation signal is superimposed on the background pressure signal, modifying it slightly at $St_e = 0.05$ (~570 Hz) and significantly at $St_e = 0.35$ (~3980 Hz), which is near the jet column or jet preferred mode Strouhal number. This mode is one of the two K–H modes and the more amplified of the two [9]. Strouhal number is merely a normalized frequency using the proper flow length and velocity scales. For a jet flow these are the nozzle exit diameter (D) and jet velocity (U_j); $St = fD/U_j$.
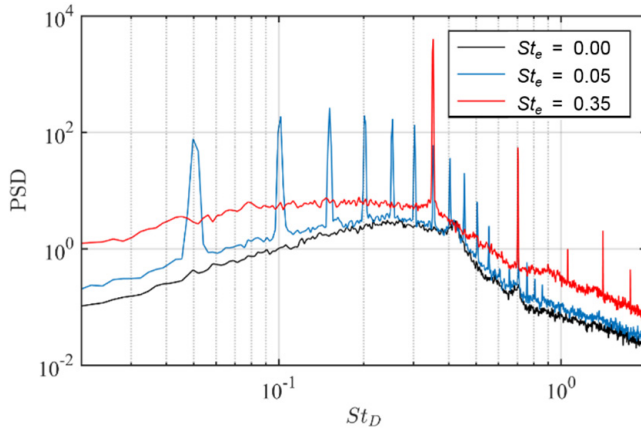
Figure 2. Near-field pressure-fluctuations spectra of an excited jet showing the fundamental actuator Strouhal number and several super-harmonics introduced by the LAFPAs. From [9]. Reprinted by permission of the American Institute of Aeronautics and Astronautics, Inc.

Strouhal number's usefulness is in its generality, as the jet preferred Strouhal number is approximately 0.3, regardless of the size or velocity of the jet. The corresponding physical frequency is ~3400 Hz for a Mach 0.9 jet and ~4600 Hz for a Mach 1.3 unheated jet, both exhausting from a 2.54 cm (1 inch) diameter nozzle. It should be noted (as mentioned above) that the physical frequency thus significantly decreases with increasing nozzle exit diameter (proportional to $1/D$).

We have successfully used LAFPAs in several high-speed, high Reynolds number flows including jets [13, 29], shock/boundary-layer interactions [35], and cavity flows [36, 37]. We will use the jet application to demonstrate the control authority of LAFPAs in high-speed and high-Reynolds number flows.

2.2. NS-DBD plasma actuators

It was first reported by Roupassov *et al* [38] that if a surface dielectric barrier discharge actuator, commonly used to impart momentum to the flow in low-speed flow control [12], is driven by a nanosecond-pulse waveform (rather than the typical AC waveform), it would generate thermal perturbations rather than induce flow velocity or momentum [17]. Such an actuator, termed nanosecond DBD (NS-DBD) actuator, has the same construction as an AC-DBD actuator as shown in figure 3(a), which includes two tape electrodes of ~0.15 mm thick each, one exposed and one covered (by the dielectric barrier), separated by a dielectric barrier tape ~0.4 mm thick, making the thickness of the actuator a fraction of a mm. Therefore, they can be pasted on a surface as shown schematically on figure 3(a). The main difference between AC-DBD and NS-DBD actuators is in the input signal, which is a high voltage (~several kV) sinusoidal waveform for the former and ~50 ns (full-width half-maximum) pulsed waveform with a similar voltage level for the latter. The difference in the input waveform makes a significant difference in the output signal and generated results, as shown in figure 3(b), which shows the induced flow velocity by the two actuators with the same geometry/setup but different input waveforms. As can be seen,
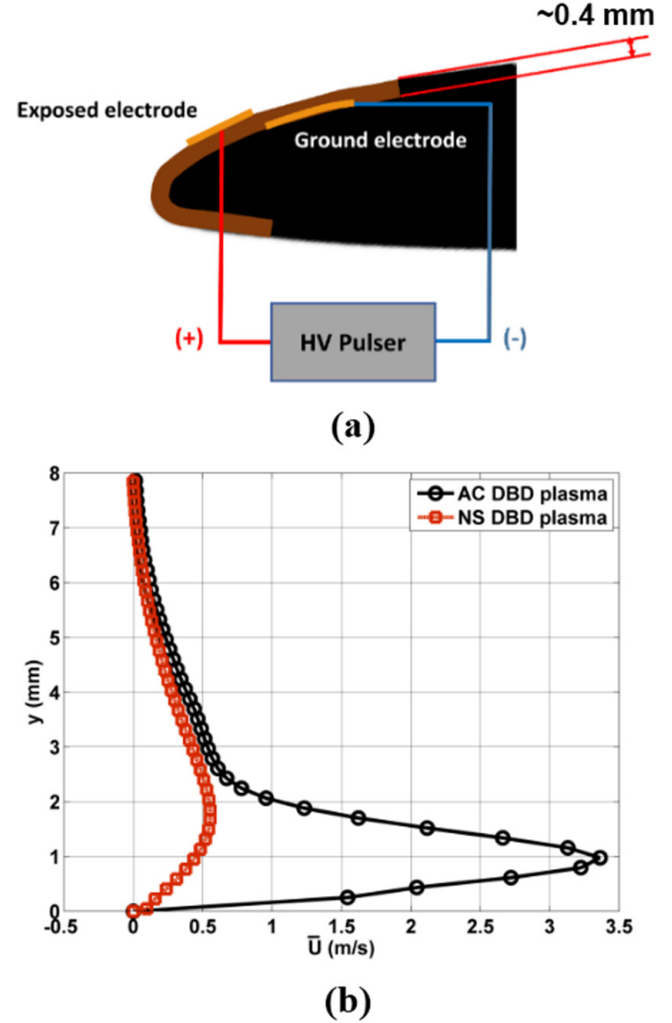

Figure 3. Schematic of an NS-DBD actuator mounted near the leading edge of an airfoil (a) and induced flow velocity by NS-DBD and AC-DBD used the same setup but different input waveform (b). (b) From [17]. Reprinted by permission of the American Institute of Aeronautics and Astronautics, Inc.

the AC-DBD actuator, which is a momentum-based actuator, can generate significantly higher velocity/momentum near the surface onto which it has been mounted, in comparison with the NS-DBD actuator, which is a perturbation-based actuator.

It should be noted that since AC-DBD and NS-DBD actuators use a near-surface discharge, some researchers have used the terms AC-SDBD and NS-SDBD. However, in the majority of publications in AFC, including the authors' own previous publications, S for the surface has been omitted. This practice is maintained in the current paper.

In terms of actuator geometry, the NS-DBD actuator is identical to the AC-DBD actuator and in terms of actuation signal (and output) it is quite similar to the LAFPAs and produces relatively high-amplitude, high-bandwidth perturbations for effective excitation of flow instabilities for control. In terms of application for flow control, the primary difference between LAFPAs and NS-DBD actuators is that while LAFPAs produce spatially-localized, discrete perturbations (and are typically used in groups of actuators distributed throughout the receptivity region, as shown in figure 1), the

NS-DBD actuators produce spatially distributed perturbations near the edge of the exposed electrode nearest the covered electrode. Recently, NS-DBD actuators have been used to control the flow over airfoils in both static stall (flow separation over a stationary airfoil) and dynamic stall (flow separation over an oscillating airfoil) conditions by manipulating the instabilities associated with the flow [17, 39–41]. Little [15] provided more details on the nature and operation of NS-DBD actuators.

As stated previously, the main mechanism through which NS-DBD actuators appear to be affecting the flow is through Joule heating. According to Adamovich *et al* [32], the heat release mechanism in a nanosecond discharge is a two-step process where the timescale of each step is significantly different from the other one. The first stage, referred to as 'rapid heating' inlvoves rapid heat release due to quenching of the N_2 excited electronic states by oxygen which happens less than 1 μs after discharge initiation. According to Aleksandrov *et al* [42], nearly half of the discharge power in this short period of time can go towards fast, localized release of thermal energy which would induce a local ΔT of about 200 K.

The next step is what commonly referred to as 'slow heating' [32] or 'delayed thermalization' [43]. The heat release during this process occurs on much longer time scales (up to several hundred microseconds after discharge initiation) and results in local ΔTs of up to 850 K. Adamovich *et al* [32] and Leonov *et al* [43] believe that this process is driven by V–T relaxation of nitrogen by O atoms. While the first step leads to generation of compression waves, the second stage results in generation of what has been referred to as 'hotspots' in the literature. Adamovich *et al* [32] believe that hotspots, thermal perturbations released over much longer timescales, are responsible for control authority of the NS-DBD actuators as compression waves are generated and dissipated over such short time scales that the flow will not be able to react to them. This assertion is supported by the numerical work of Zheng *et al* [44].

Similar to LAFPAs discussed above and shown in figure 2, the impulsive nature of the NS-DBD input waveform results in the introduction of perturbations not only at the fundamental actuation frequency, but also at several super-harmonics. Figure 4 shows near-field pressure-fluctuation spectra measured using a microphone just outside of the separated region in a flow over an installed Boeing VR-7 airfoil for the baseline flow and four excited cases [45]. The pressure fluctuations outside of the separated flow zone are generated by flow structures in the shear layer over the separated zone that are formed due to the K–H instability and convected downstream. However, the pressure amplitude drops exponentially from the source (i.e. large-scale structures) to the microphone [34]. Therefore, the relative amplitude of peaks in a given case is important, but the absolute amplitude of the peaks in different cases cannot be accurately compared. In the baseline case, there is a peak at Strouhal number of 0.6 (110 Hz), which is associated with the shedding of natural flow structures from the shear layer into the wake of the airfoil. By way of reminder, the Strouhal number ($St = fc/U_\infty$) is a nondimensional frequency. For this application the appropriate length and velocity scales are airfoil chord length (*c*), and flow freestream velocity (U_∞). As in
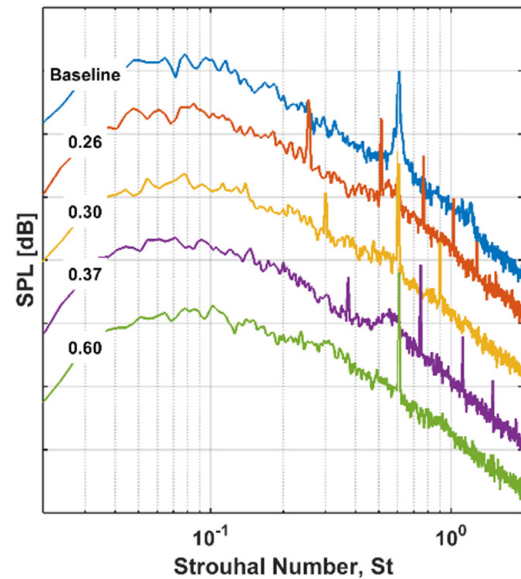

Figure 4. Near-field pressure-fluctuations spectra for the baseline and excited cases at 4 different Strouhal numbers (0.26 (44 Hz), 0.30 (55 Hz), 0.37 (68 Hz), and 0.60 (110 Hz)) measured in a stalled airfoil flow in a fixed location outside the separation zone. Each spectrum is offset by 10 dB for readability.

the jet case, its usefulness is in its generality, as the shedding Strouhal number is ~1, regardless of the size of the airfoil or speed of the flow.

There are several peaks for each one of the three excited cases, but the peak closest to the natural shedding Strouhal number in each case has the highest amplitude. As was mentioned earlier and will be further discussed later, the K–H instability has two modes in flows such as jets and separated flows. The lower frequency mode is associated with the shedding frequency in the baseline case and is the more amplified of the two [9]. Similar actuator-produced perturbations, i.e. the fundamental frequency along with several super-harmonics, have been reported by Visbal [46–48] in large-eddy simulations where periodic blowing and suction (with a step function profile) for flow separation control was employed.

Thermal-based actuators for excitation of instabilities (LAFPA and NS-DBD) have ushered in the most recent developments in AFC, whereby significant gains can be achieved using relatively small inputs. The high-bandwidth, high-amplitude perturbations these devices generate, and their flexibility, have not only opened the possibility of excitation of natural flow instabilities in previously inaccessible high-speed, high Reynolds number flows, but have also allowed optimization and feedback control in both these and other flows. The flow control community has now been exploring these exciting new areas for over a decade. In what follows, a brief discussion of shear-flow instabilities will be provided before a presentation of sample results in jet flows using LAFPAs and in flow over an airfoil using NS-DBD plasma actuators.

3. Instability in free shear flows

Free-shear flows in which shear layers are formed away from any adjacent surface are ubiquitous in aerospace applications.

They include jets and cavity geometries of any size and separated flows of any kind. Free-shear flows are known to be amenable to excitation and can amplify any naturally-present or artificially-seeded thermal, acoustic, or hydrodynamic perturbations over a wide range of frequencies. Observations of this instability date back to the 19th century when, for example, Leconte [1] noticed that the flame of a gas burner was swaying to the beats of classical music. However, mathematical formulation of this instability did not take place until mid-1960s when Michalke [2–4] explored details of this instability, which is termed the Kelvin–Helmholtz (K–H) instability. He showed that the K–H instability can amplify small perturbations over a wide range of frequencies and lead to the formation of large-scale structures [3]. It is known that the dynamics of these structures dominate important processes in turbulent flows, such as entrainment, mixing, momentum and heat transport, and noise generation. Crow and Champagne [5] showed that axisymmetric free-shear flows or jets can act as a band-pass amplifier and generate and support coherent large-scale flow structures. Brown and Roshko [6] serendipitously discovered the existence of coherent large-scale flow structures in high Reynolds number planar (2-D) free shear flows while they were investigating the effect of density in mixing layer growth rate. These findings spurred tremendous activities in the 1970s and 1980s in the use of AFC not only to excite flow instabilities but also to better understand the physics of large-scale flow structures. Ho and Huerre [8] covered most of the developments made until the mid-1980s and Samimy *et al* [9] those made thereafter.

The initial, higly simplified, instability analysis assuming non-diverging free-shear layers (i.e. shear layer with negligible growth) was followed by increasingly more realistic and involved analyses, including using slowly diverging free-shear layers [49, 50], linear parabolic stability equations [51, 52], and optimal disturbance technique with a fully non-parallel frame work [53]. While there are differences in the details of the results obtained using various analyses, all these studies confirmed that linear K–H instability, which is essentially an inviscid instability (i.e. with negligible viscous effects) in aerospace applications with high Reynolds number, governs the initial growth of perturbations. A more detailed discussion of these issues can be found in Samimy *et al* [9]. Some important, but relatively less understood issues in the literature, which are pertinent to AFC and excitation of flow instabilities will be briefly discussed below.

The earlier K–H instability work focused on a simple 2-D model (i.e. a shear layer formed downstream of a splitter-plate separating two flows of different velocities). When the two flows merge at the trailing edge of the splitter plate, a free-shear layer is formed. This free-shear flow has a single length scale, the local momentum thickness (θ) of the shear layer, which increases in the streamwise direction. While the shear layer can amplify perturbations over a wide a range of frequencies, the maximum amplification of perturbations normally occurs at a Strouhal number $St_n = f_n\theta/U_{ave} \sim 0.032$ [8], where f_n is the most amplified frequency, U_{ave} is the average velocity of two streams, and θ, as defined above, is the local momentum thickness. In practical applications with more complex geometries,

there is often a second length scale, which typically plays an even more important role in the growth of perturbations and the development of ensuing large-scale flow structures than the local momentum thickness. This length scale is, for example, the nozzle exit diameter in jets, the length of the separated zone in separated flows, and the cavity streamwise length in cavity flows. In flows with no excitation, the observed flow structures are typically associated with this length scale and the frequency associated with these structures is called by different names in different flows. For example, in jets it is called 'jet-column mode' or 'jet-preferred mode' (with $St = fD/U_j \sim 0.3$, where D is the nozzle exit diameter and U_j is the nozzle-exit centerline velocity) and in a stalled flow over an airfoil it is called 'natural shedding frequency' (with $St = fc/U_\infty \sim 1.0$, where c is the airfoil chord length and U_∞ is the freestream velocity). While it has not been clear in the literature, the two frequencies associated with these two length scales are two modes of the K–H instability, as Hussain [54] asserted. In jets, the two modes are called the shear-layer mode and the jet-preferred mode. More detailed information on this issue can be found in Samimy *et al* [9]. The significant differences between these two modes will be abundantly clear when we present some experimental results on two example problems.

In the next two sections, experimental results from two example practical problems of very different nature will be presented and discussed. The flow is excited using the two plasma actuators discussed above, namely LAFPAs and NS-DBDs. Many of the issues examined so far will be revisited in the discussion of these results.

4. Experimental results in two different flows using plasma actuators

4.1. Sample AFC results in high-speed jets using LAFPAs

Jets of all sizes are used in aerospace applications, from micro thrusters in space applications to large exhaust jets in commercial aircraft. Some results obtained from a jet exhausting from a 1 inch (2.54 cm) diameter axisymmetric nozzle are presented in this section. The facility can generate cold or heated (up to 800 K) subsonic and supersonic jets with Reynolds numbers of up to 2×10^6, depending upon the Mach number and temperature [9]. Figure 5 shows two images of a Mach 1.3 jet. The images are obtained using a laser sheet, which is passed through the centerline of the jet and the light is scattered by condensed moisture particles of ~ 1 μm diameter that are formed in the mixing layer between the jet and the ambient air. The jet exhausting from the nozzle is dry, cold air with no moisture and the warmer, moist, ambient air is entrained into the mixing layer of the jet by large-scale flow structures in the mixing layer (or shear layer). During the mixing process, moisture in the entrained ambient air condenses into water droplets in the mixing region, which scatter the laser light and thus visualize the mixing region of the jet. Figure 5(a) is an ensemble-averaged image of the baseline jet and figure 5(b) is a phase-averaged image of the jet controlled by 8 LAFPAs operating in-phase (axisymmetric mode, $m = 0$) at a Strouhal number ($St_e = fD/U_j$) of 0.33. The significance

J. Phys. D: Appl. Phys. **52** (2019) 354002

M Samimy *et al*

of this Strouhal number has been discussed above and will be reexamined later. In the baseline jet, coherent, large-scale flow structures are formed due to the amplification of natural perturbations in the flow and can be observed (not shown here) in the instantaneous images of the shear layer. However, they appear in a random fashion (both temporally and spatially) in the mixing layer and thus become indistinguishable after the ensemble-averaging process. On the other hand, the more coherent flow structures in the controlled case are organized and in-phase with the actuation signal and are highlighted by the phase-averaging process. In the radial cross-section of the jet (not shown here), the flow structures or vortices appear as rings in the mixing layer of the jet and grow both outward and inward, resulting in the disappearance of the jet core by the end of the potential core (and the rings become disks), which is approximately 5D to 6D downstream of the nozzle exit. The end of potential core is where the process of structure break up and disintegration begins and far-field peak noise in commercial and military aircraft is generated [9, 55]. This issue will be further discussed later in the paper.

Figure 6 shows the effects of varying the excitation Strouhal number (nondimensionalized frequency) on the flow structures observed in figure 5. The excitation azimuthal mode is no longer the axisymmetric mode ($m = 0$) shown in figure 5, where the structures are symmetric, but now it is the flapping mode ($m = \pm 1$, which can be obtained by superimposing the two first helical modes spinning in clockwise and counterclockwise directions) where the structures are asymmetric with respect to the jet streamwise axis. It is well known in the literature that axisymmetric jets respond to various azimuthal modes and with eight actuators one could excite $m = 0, 1, 2, 3,$ and ± 1 (axisymmetric, first, second, and third helical, and flapping, respectively) modes and a couple of additional mixed modes ($\pm 2, \pm 4$). In figure 6, a phase-averaged velocity field obtained using particle image velocimetry (PIV) is used to calculate the Galilean streamlines [56] as well as Q-Criterion [57] (a vortex identification metric) to better visualize the flow structures, including both structure core (cyan color) and braid (magenta color) regions. As can be readily observed, the flow structures become much smaller and their development and disintegration occur further upstream in the jet as the excitation Strouhal number is increased from 0.33 (~5.08 kHz) in figure 6(a) to 1.05 (~16.16 kHz) in figure 6(b). It is well known that the interaction and disintegration of large-scale structures in jets (beginning just upstream of the jet potential core) generate the peak far-field noise [55], which has been a major topic of research since the inception of jet engines. The interaction and breakdown of these smaller structures is much gentler, and thus the far-field peak noise is reduced when the structures become smaller [58]. This issue will be further discussed later.

The results in figures 7 and 8 demonstrate the effects of excitation of flow instability on the global characteristics of a jet. Figure 7 shows the effect of excitation Strouhal number on the growth of a Mach 0.9 jet, which is defined as the changes in the jet width (twice the radial distance of the half-centerline velocity location at a given *x/D*) [58]. The results are shown for the baseline jet and two excitation cases associated with
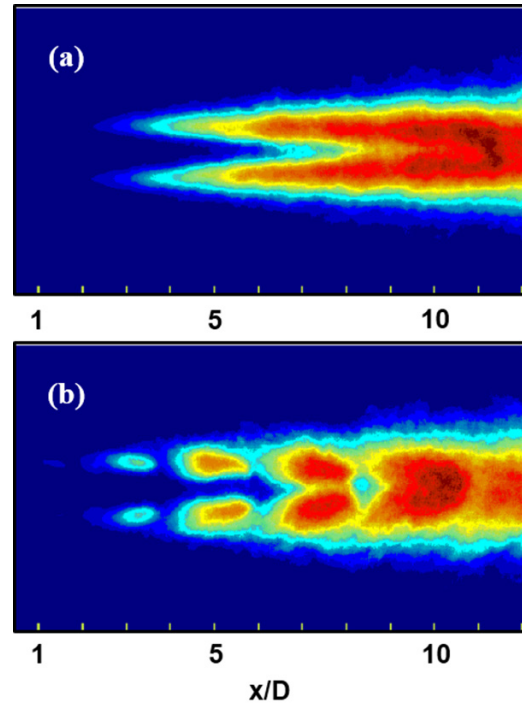

Figure 5. Streamwise planar visualization of the mixing layer of a Mach 1.3 axisymmetric jet. *X* is the streamwise distance from the nozzle exit and D is the nozzle exit diameter. Ensemble-averaged image of the baseline jet (a) and phase-averaged image of the jet excited at a Strouhal number of 0.33 (5.08 kHz) (b) are shown. White tick marks correspond to 1 jet diameter increments of the streamwise coordinate.

the two different K–H modes: one low Strouhal number case (near the jet-preferred mode) associated with the nozzle exit diameter as the length scale and one high Strouhal number case (near the shear-layer mode) associated with the shear layer momentum thickness as the length scale. The jet responds over a band of Strouhal numbers around each of these two modes: from $St_e = 0.2$ to 0.6 for the jet-column mode [59] and an order of magnitude higher St_e and an even larger band for the shear-layer mode [9]. The low and high Strouhal number excitations significantly increase and decrease, respectively, the jet growth, as defined above. These results are consistent with the results shown in figure 6, which demonstrated the effects of excitation St_e on the size and development of large-scale structures. Large-scale structures are known to dominate the mixing, entrainment, heat and momentum transport, and noise generation processes—the more coherent and larger structures produce more mixing and entrainment as well as increased peak far-field noise (discussed more later). As a result, the choice of excitation St_e depends on the objective of the control (e.g. mixing enhancement or noise suppression).

Figure 8(a) shows jet noise (sound pressure level, SPL) spectrum in the far field of a hot Mach 1.3 jet (measured at a distance of more than 70D away from the jet) [60, 61]. The abscissa and ordinate show the microphone-location angle (called polar angle) with respect to the jet axis and SPL Strouhal number, respectively, and the color bar shows the SPL. It has been known since 1950s that the jet noise level scales approximately with the jet velocity to the 8th power [62], which means a hotter/higher velocity jet produces
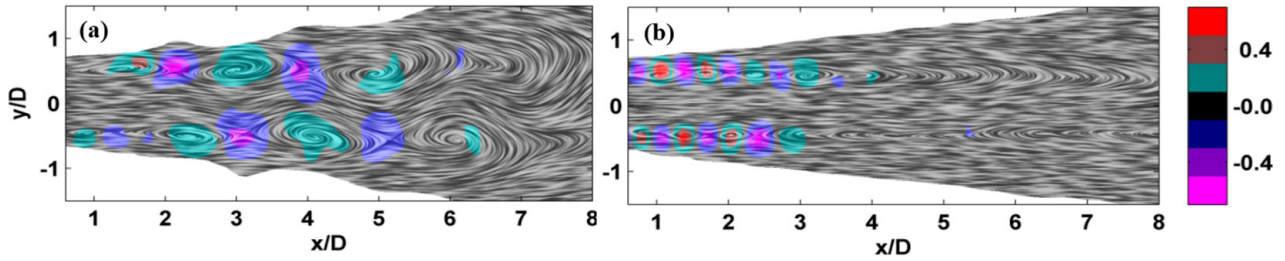
Figure 6. Galilean streamlines superimposed on maps of Q-Criterion (a vortex detection metric) demonstrating the effects of excitation Strouhal number (normalized frequency) on the large-scale flow structures of a Mach 1.3 jet with Re_D of 1.1×10^6 using the flapping azimuthal mode ($m = \pm 1$). Strouhal numbers of 0.33 in (a) and 1.05 in (b) correspond to 5.08 kHz and 16.16 kHz, respectively.
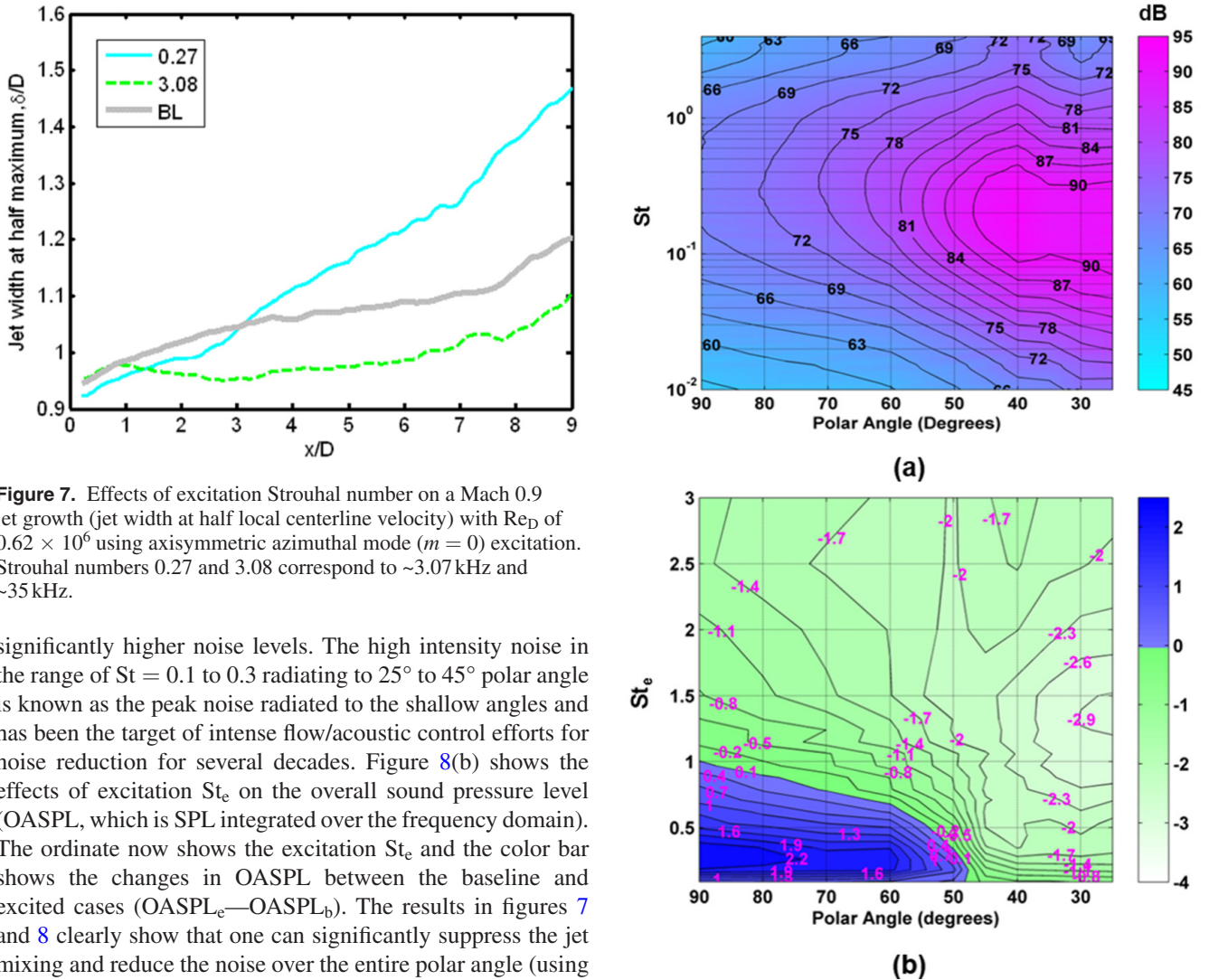

Figure 7. Effects of excitation Strouhal number on a Mach 0.9 jet growth (jet width at half local centerline velocity) with Re_D of 0.62×10^6 using axisymmetric azimuthal mode ($m = 0$) excitation. Strouhal numbers 0.27 and 3.08 correspond to ~3.07 kHz and ~35 kHz.

significantly higher noise levels. The high intensity noise in the range of St = 0.1 to 0.3 radiating to 25° to 45° polar angle is known as the peak noise radiated to the shallow angles and has been the target of intense flow/acoustic control efforts for noise reduction for several decades. Figure 8(b) shows the effects of excitation St_e on the overall sound pressure level (OASPL, which is SPL integrated over the frequency domain). The ordinate now shows the excitation St_e and the color bar shows the changes in OASPL between the baseline and excited cases ($OASPL_e$—$OASPL_b$). The results in figures 7 and 8 clearly show that one can significantly suppress the jet mixing and reduce the noise over the entire polar angle (using high-frequency excitation of jet instability) or enhance the mixing and thus reduce the noise in some angles and increase it in some other angles (using low-frequency excitation of jet instability), depending upon the choice of excitation St_e. In some recent publications, Kopiev *et al* [63, 64] have also used three different types of surface discharge plasma actuators to control jet noise using excitation of flow instability.

To further illustrate the power of AFC using excitation of flow instability, figure 9 shows results from a Mach 1.3 twin-jet, exhausting from two side-by-side bi-conical converging-diverging nozzles separated from each other by 2 nozzle exit diameters (centerline-centerline) [65]. This twin-jet apparatus

Figure 8. Far-field noise (SPL) spectrum of a baseline Mach 1.3 hot jet (a) and the effects of excitation Strouhal number on the OASPL (b).

uses the same facility as the single jet discussed earlier. Each nozzle has an exit diameter of 0.75 inch (1.905 cm). Several current military aircraft use such an arrangement. In a twin-jet configuration, the jets can interact and couple, not only significantly increasing the far-field radiated noise but also the near-field pressure fluctuations, which can damage nearby aircraft surfaces. Figures 9(a) and (b) show the schlieren image and near-field SPL spectrum of the baseline twin-jet. As can
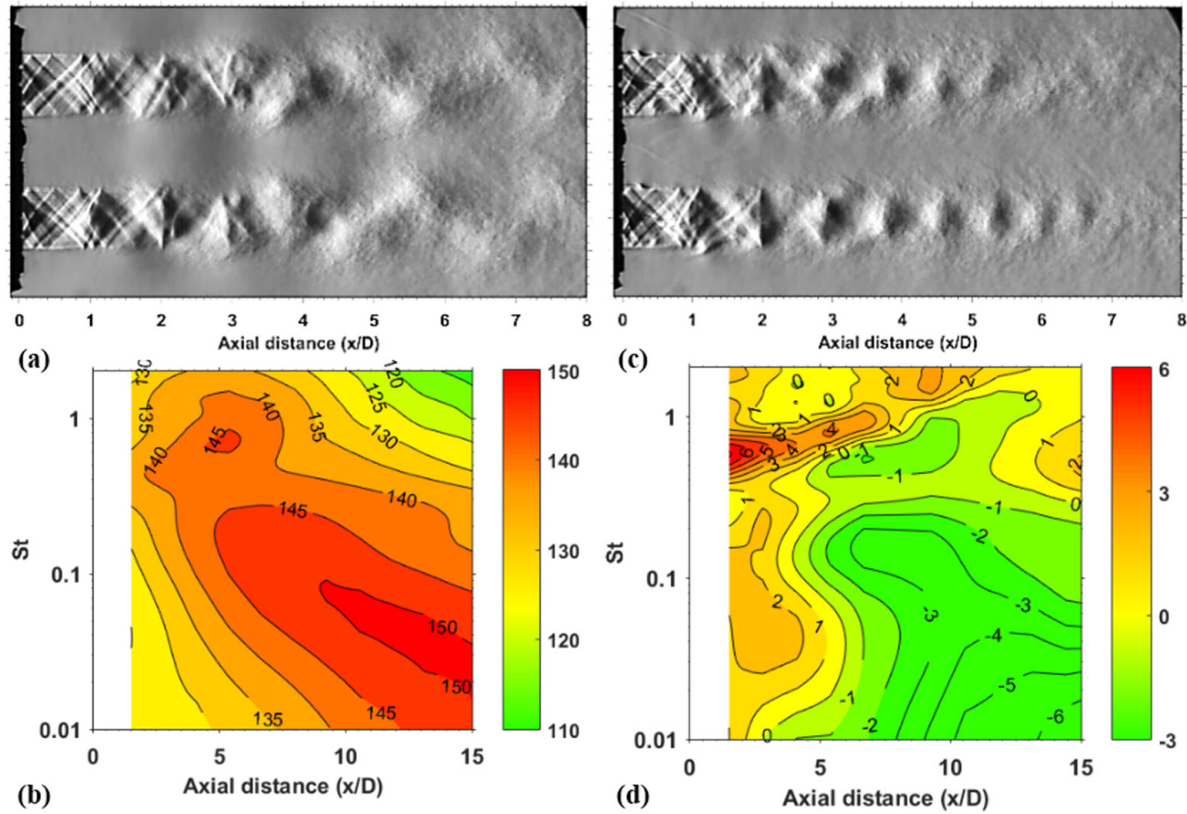
J. Phys. D: Appl. Phys. **52** (2019) 354002

M Samimy *et al*

Figure 9. Schlieren image (a) and near-field SPL spectrum (b) for a baseline Mach 1.3 axisymmetric twin-jet and the effect of excitation ($St_e = 0.3$ (~6.16 kHz), $m = 3$) on the flow structure (c) and the changes in the near-field SPL with respect to the baseline case (d).

be seen in the schlieren image, the two jets are coupled and operate in symmetric flapping mode (both jets move synchronously towards or away from the other jet) generating significant near-field SPL at low Strouhal numbers. Figure 9(c) shows the schlieren image of the jets excited with $St_e = 0.3$ (~6.16 kHz) at 3rd helical mode ($m = 3$). The control completely eliminates the jet-jet interaction. This is because the excitation of the jet instability has replaced the natural, large-scale structures responsible for the coupling with much smaller, azimuthally incoherent structures. Figure 9(d) shows the changes in the SPL between the baseline and excited twin-jet (SPL_e—SPL_b). As can be seen, the intense SPL in low frequencies has been reduced by as much as 6 dB.

The measured instantaneous current, voltage, and power dissipation are all quite high in LAFPAs [9, 13, 14]. However, the low (20%) duty-cycle (i.e. short pulse-width), each actuator consumes a time-averaged power of approximately 20 W. With AFC using 8 actuators, consuming approximately 160 W of power, flow structures, near-field pressure, and far-field radiated noise of a supersonic jet issuing from a 2.54 cm nozzle can be tailored at will. This is a textbook definition of AFC with $O(\varepsilon)$ input and $O(1)$ response. Scaling up to application sizes is actually beneficial in these applications, as for example, the jet power increases with D^2 while the number of actuators increases linearly with D (nozzle exit diameter). However, for these actuators to get on flight vehicles, many further advances must be achieved, paramount among them are miniaturization of the power supply, improvement in thermal efficiency, and reduction of electromagnetic

interference, which could interfere with onboard electronics and communication systems. In addition, the initial applications must be carefully chosen to generate success stories, thereby motivating further developments to be pursued.

4.2. Sample AFC results in separated flows using NS-DBD plasma actuators

Flow separation occurs in many aerospace applications, especially over lift-generating surfaces (e.g. airfoils) when the angle of attack (α) is increased beyond the stall angle, which depends on the surface geometry and flow Reynolds number, among other flow properties. Flow separation can cause significant detrimental effects, including loss of lift and increased unsteady forces leading to structural fatigue. While flow separation control utilizing passive techniques has been used from the dawn of aviation, AFC for separation control has only been the subject of intensive research over the past few decades. Vibrating surfaces, acoustic devices, and fluidic actuators have all been used for active control of separation, but fluidic actuators which inject momentum into the flow have been the most commonly used AFC technique for flow separation control [16]. Flow separation control using plasma actuators, especially AC-DBD actuators (which also inject momentum into the flow) has been widespread [12, 20, 21]. However, as was discussed earlier, the momentum generated by these actuators is relatively small, and thus their application is limited to flows with speeds less than about 50 m s^{-1}.
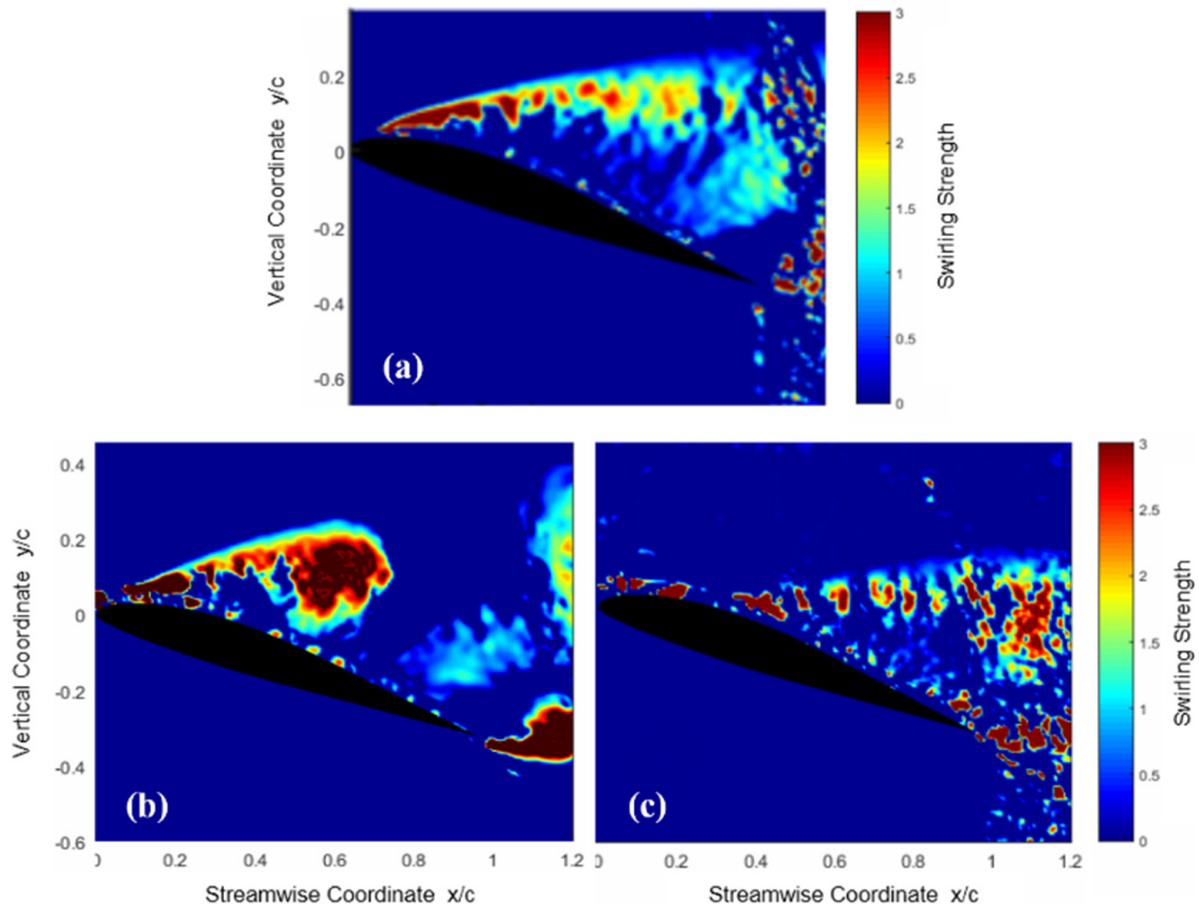
Figure 10. Phase-averaged flow structures (visualized using swirling strength) for the baseline post-stall flow over a VR-7 airfoil (a) and effect of excitation on the flow structures at $St_e = 0.6$ (~110 Hz) (b) and 6.0 (~1100 Hz) (c).

Over the past 15 years, NS-DBD actuators, which generate thermal perturbations rather than momentum (as shown in figure 3), have been used for flow separation control over airfoils [17, 39, 41, 45]. However, there has been a general lack of understanding on the actual control mechanism of NS-DBD actuators. As was discussed earlier and shown in figure 3, the physical configuration of NS-DBD and AC-DBD actuators is identical, but the input voltage for the former has an alternating current waveform and for the latter a pulsed waveform of less than 50 ns full-width half-maximum duration. While details of the actuators' geometry and output signals are quite different, the overall output of NS-DBD actuators and LAFPAs, as far as the flow is concerned, is a thermal perturbation. There is, however, one major difference between the two outputs. The amplitude of the perturbation for LAFPAs is localized and significantly higher than that of NS-DBD actuators, which have a distributed output. These differences make them suitable for different flows.

In this section, sample results from flow separation control over an airfoil using an NS-DBD actuator will be presented and discussed. The airfoil is a Boeing VR-7 airfoil with an 8 inch (20.32 cm) chord length. This is an asymmetric airfoil typically used in rotorcraft applications. Figure 10 shows phase-averaged flow structures, visualized using swirling strength calculated from PIV results [56], over a fully-stalled Boeing VR-7 airfoil in the baseline and two controlled cases. Swirling strength is one of several techniques used in fluid dynamics to visualize flow structures using PIV measurements. The Reynolds number (Re = $U_\infty c/\nu$; U_∞, c, and ν being freestream velocity, airfoil chord length, and kinematic viscosity, respectively) is 5×10^5, α is 19°, while the stall angle for this airfoil at this Reynolds number is about 17°, and the flow is left to right [45]. For the baseline case shown in figure 10(a), a microphone was placed outside the shear layer formed over the separated zone in the near-field acoustic/pressure region, to detect hydrodynamic pressure fluctuations due to passage of flow vortices (see figure 4). The signal was then used as a reference for phase-locking. For the excited cases, the actuator trigger signal was used for phase-locking.

For the baseline case, the natural perturbations in the flow are amplified by the shear-layer Kelvin–Helmholtz instability and generate large-scale flow structures. In this case, the second K–H mode associated with the airfoil chord length c ($St_e = fc/U_\infty$) amplifies the natural perturbations [9]. These structures entrain the high-momentum free-stream air into the shear layer while developing and convecting over the airfoil and eventually shedding into the wake, with St = 0.6 (~110 Hz) as shown in figure 4. The structures are phase-locked with the vortex shedding from the trailing edge. When the flow is excited at the natural shedding frequency ($St_e = 0.6$, ~110 Hz), the large-scale structures in the shear layer are significantly more coherent, as seen in figure 10(b),
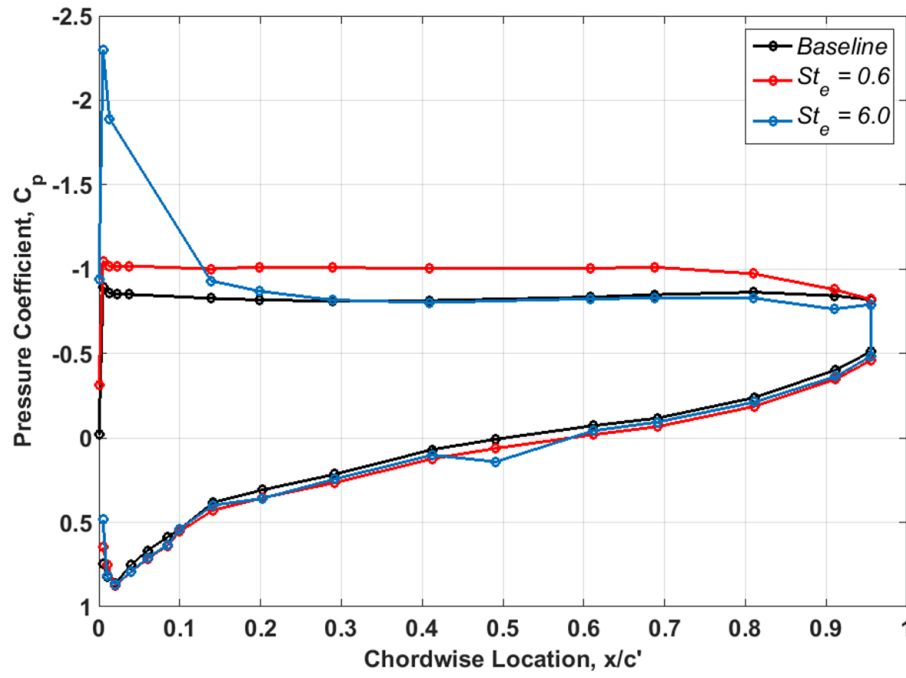
Figure 11. Pressure coefficient distribution for the baseline and two excited cases shown in figure 10 at $\alpha = 19°$ and Re $= 0.5 \times 10^6$. Strouhal numbers 0.6 and 6.0 correspond to ~110 HZ and ~1100 Hz.

due to injection of coherent perturbations with a well-defined frequency. In addition, the actuator trigger signal for phase-locking of the data acquisition is much sharper (well defined) than the near-field pressure signal used to track and lock the data acquisition to the baseline flow structure shedding. Thus, the significant increase in coherency of the flow structures in the excited case in comparison with those in the baseline case is due to a combination of these two factors. When St_e is increased by an order of magnitude in figure 10(c) ($St_e = 6.0$, ~1100 Hz) into the K–H shear-layer mode band, the flow structures become much smaller, less coherent, and their development and disintegration occurs much further upstream over the airfoil. In this case, the flow is attached over 1/3 of the airfoil.

In the baseline and the low St_e excitation cases, the time-averaged flow is fully separated over the airfoil, resulting in loss of the lift. However, as a structure is developing and convecting in the shear layer over the separated region, due to the K–H instability's second mode, it entrains the high-momentum ambient air into the separated zone and reattaches the flow until it sheds from the trailing edge. The flow then returns to the separated stage, which marks the end of one and beginning of another cycle. As a result, the flow goes through cyclic separation and reattachment processes, which generate significant, unsteady, cyclic forces on the airfoil.

Figure 11 shows the time-averaged surface pressure results over the airfoil for the three cases shown in figure 10. For the baseline and the low St_e excitation cases, the pressure distribution over the airfoil is flat, indicating the cyclic separation and reattachment of the flow. However, the suction generated by the excited case is significantly higher, as the more coherent structures shown in figure 10(b) (in comparison with those of the baseline case) can entrain more high-momentum
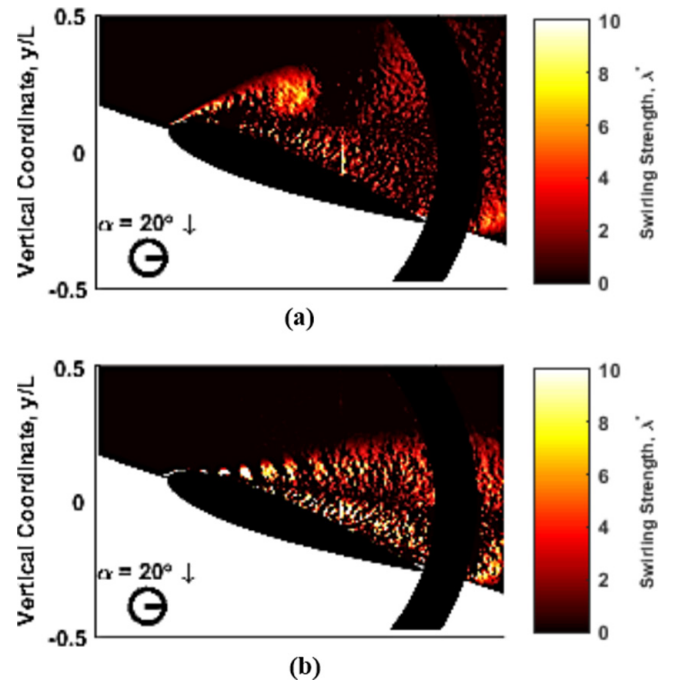

Figure 12. Plots of normalized swirling strength demonstrating the effects of excitation Strouhal number on the phase-averaged flow structures in the down-stroke of an oscillating NACA 0015 airfoil at excitation Strouhal numbers of $St_e = 0.35$ (~39 Hz) (a) and 9.9 (~1090 Hz) (b).

free-stream fluid into the mixing region. This better reattaches the flow, and therefore increases the suction over the airfoil. As St_e is increased by 10-fold, the structures become much smaller, but more frequent, and their development moves further upstream on the airfoil, as shown in figure 10(c). As a result, they generate a significantly larger suction peak over
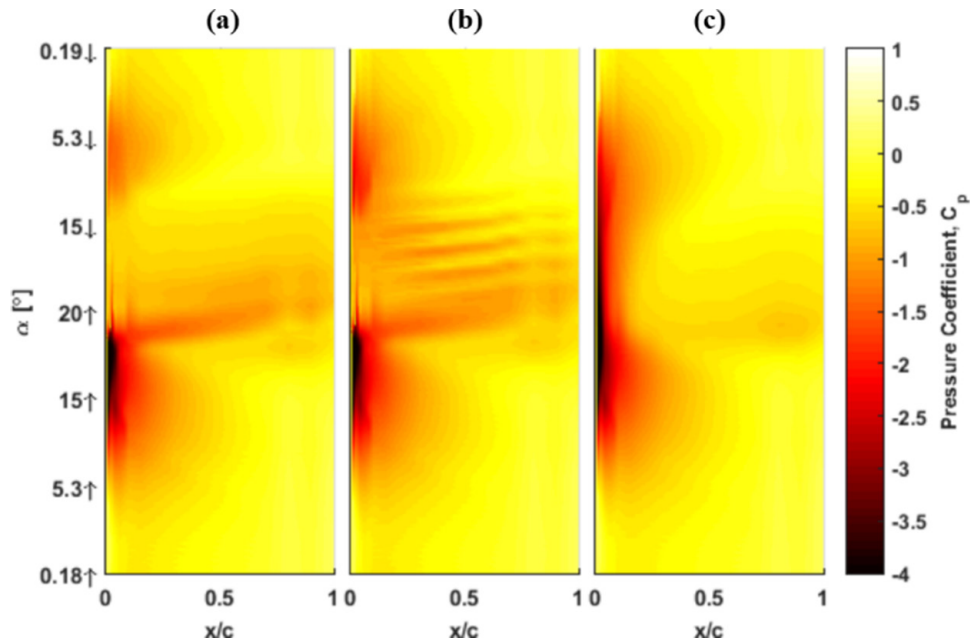
Figure 13. Phase-averaged pressure coefficient over one complete cycle on the suction surface for the baseline oscillating NACA-0015 airfoil (a) and the excited cases at $St_e = 0.35$ (b) and 9.9 (c). Strouhal numbers of 0.35 and 9.9 correspond to ~39 Hz and ~1090 Hz).

about the upstream 1/3 of the airfoil. Since most of the lift in the VR-7 airfoil is generated near the leading edge, the high St_e significantly increases the lift. Note that this is observed in spite of the fact that the three (out of 33 total) closest surface pressure taps to the leading edge of the airfoil are covered by the plasma actuator. Given that the flow is fully separated (as can be inferred from the flat suction-surface pressure distribution in figure 11) in the baseline and low St_e cases, the loss of pressure taps is of little consequence for these two cases. However, for the high St_e case, due to the increased suction peak close to the leading edge, the coefficient of lift would be underestimated. It is for this reason that only the coefficient of pressure, rather than lift distributions, are shown in figure 11. The pressure coefficient is defined as $C_p = (p - p_\infty)/q_\infty$, where p, p_∞, and q_∞ are static pressure at the measurement location on the airfoil surface, freestream static pressure, and freestream dynamic pressure, respectively.

To demonstrate the robustness of the AFC technique using thermal perturbations generated by plasma actuators, sample results from AFC using an NS-DBD actuator in a flow over an oscillating airfoil, which is quite a complex flow, is briefly discussed here. The airfoil has a symmetric NACA 0015 profile having a chord length of 8 inches (20.32 cm) operated at a Reynolds number and reduced frequency ($k = \pi f c/U_\infty$, f being the oscillation frequency) of 3×10^5 and 0.05, respectively. Using lower and higher Re numbers (1.67×10^5 and 5×10^5) and k (0.025 and 0.075) resulted in similar trends as will be shown and briefly discussed below [40]. The airfoil at this Reynolds number stalls at an α of around 13°. The oscillation angle varied from 0 to 20°. It has been known that in oscillating airfoils, α can significantly increase beyond the static stall α before the airfoil dynamically stalls. During this process, significant vorticity accumulates at the leading edge of the airfoil. This vorticity is eventually dislodged in the form of a large flow structure called the dynamic stall vortex

(DSV). Similar to large-scale flow structures shedding in the static stall case, DSV momentarily attaches the flow while convecting over the airfoil, but the flow separates after the DSV convects beyond the trailing edge. This generates significant unsteady forces, which is undesirable. In the results shown below, the baseline dynamic stall angle was 19.6°.

The excitation St_e ($St_e = f c/U_\infty$) was varied from 0 to 10 (0 to ~1100 Hz), covering both K–H mode bands. Figure 12 shows phase-averaged flow structures (visualized using swirling strength) for the excitation around these two modes right after the airfoil has reached the highest α and started the down-stroke motion. The DSV is enhanced and clearly visible at the lower St_e case, while in the high St_e case it has been replaced by much smaller flow structures. In addition, the flow is attached for the high St_e case over part of the airfoil and the separation region has been significantly reduced over the entire airfoil. Basically, the high St_e excitation gradually bleeds the accumulated vorticity (by triggering the generation of structures) and completely eliminates the DSV. The flow responds over the entire range of tested excitation Strouhal numbers and the response changes gradually from one to the other displayed case [40].

Figure 13 shows plots of phase-averaged pressure coefficient over one complete oscillation cycle for the NACA 0015 airfoil for the baseline and two excited cases. The baseline case (figure 13(a)) clearly shows the significant increase in the suction pressure (negative pressure coefficient) as α increases beyond the static stall angle of 13° until the flow separates just before reaching α of 20°. The results also show the increase in the suction due to the DSV, as it convects over the airfoil, and (in the down-stroke phase) when the flow reattaches. Excitation at the low St_e of 0.35 (~39 Hz) (figure 13(b)), within the band of the K–H instability's second mode, enhances the DSV, as shown in figure 12. It also increases the suction in the reattachment phase of the down-stroke when large-scale

structures formed in the shear layer over the separated zone are convected over the airfoil and momentarily reattach the flow. Excitation at a much higher St_e of 9.9 (~1090 Hz) (figure 13(c)), within the band of the K–H instability's shear-layer mode, completely eliminates DSV, as shown in figure 12(b). In addition, it increases the suction near the airfoil leading edge over nearly the entire down-stroke phase. One of the most important advantages of high St_e excitation is the significant reduction in unsteady forces exerted by the flow on the airfoil [40].

5. Concluding remarks

This paper focuses on a class of flows that are present in many aerospace and other applications. They are unstable to flow perturbations (thermal, acoustic, and hydrodynamic) over a large-range of frequencies, making them amenable to and an excellent target for AFC. Some applications include jets, cavity flows, and separated flows of any kind. All these flows include a free shear layer, i.e. a shear layer far from any solid surface. The instability, called the Kelvin–Helmholtz (K–H) instability, has two modes associated with two length scales of the flow. There is an order of magnitude difference in scale between the two. Excitation at frequencies targeting both modes provide opportunities for AFC with different control objectives, for example, mixing enhancement or noise mitigation in jet applications.

Theoretical basis for the K–H instability was established in 1960s and 1970s and large-scale flow structures developed in the flows due to this instability were discovered in 1970s. Owing to the importance of large-scale structures, which are responsible for important processes such as mixing, momentum and heat transport, noise generation, etc, AFC in such flows flourished in the 1970s and 1980s. The actuators used were of mechanical, fluidic, and acoustic type. Unfortunately, the AFC research activities were limited to low-speed and relatively low-Reynolds number flows due to limitations of these actuators. As the flow speed and Reynolds number rise, so do the background turbulence and instability frequencies, requiring high-amplitude, high-bandwidth perturbations to excite the flow instabilities. These two opposing requirements impose a significant demand on the mechanical, fluidic, and acoustic actuators then in use. Acoustic actuators meet the former while the two others meet the latter requirement. As a result, there was practically no experimental work in the active control of high-speed and high Reynolds number free-shear flows.

Development of two classes of plasma actuators over the past 15 years, namely LAFPAs and NS-DBD plasma actuators, has energized AFC activities in free-shear flows of interest in aerospace applications. Therefore, the focus of this paper is on the application of these two well-known classes of plasma actuators to control flows with the K–H instability and wide-ranging aerospace applications (thus, 'reinventing the wheel' in the title). These two actuators were briefly discussed in section 2 and a brief introduction to the shear-layer instability was provided in section 3. These actuators simply

provide thermal perturbations at frequencies within the range of the unstable frequencies of the flow instabilities. The flow takes the perturbations and amplifies them, generating large-scale flow structures. Since these structures dominate the most important processes in the flow (e.g. entrainment, mixing, momentum and heat transport, and noise production), the AFC provides an incredibly powerful means of changing the nature of these flow structures, and thus these processes. Further, since the technique is to excite instabilities in the flow rather than directly control it, the power consumption is very small, making it extremely attractive for AFC.

Sample results using instability-based AFC in two very different flows using these two actuators of very different construction and characteristics were presented and discussed in section 4. These results clearly demonstrate the control authority of the actuators in very different flows and their potential for significantly changing the nature and behavior of flows with a relatively small energy use. In addition to flow control, these actuators provide an excellent means of further exploring and understanding flow structures and physics.

While these actuators are excellent tools in a laboratory environment for AFC, they require further development to move from laboratory to application, especially aerospace applications. Both of them, especially the LAFPAs, generate a significant amount of electromagnetic inference, which could affect electronics and communications on an aircraft. In addition, their power supplies must be made more efficient and compact for application. Further, they must operate fail-safe, i.e. in all weather conditions.

Acknowledgments

ORCID iDs

Mo Samimy ● https://orcid.org/0000-0003-0234-9655
Ata Esfahani ● https://orcid.org/0000-0001-5087-2921

References

[1] Leconte J 1858 On the influence of musical sounds on the flame of a jet of coal-gas *Phil. Mag.* **15** 2035–9
[2] Michalke A 1965 On spatially growing disturbances in an inviscid shear layer *J. Fluid Mech.* **23** 521–44
[3] Michalke A 1965 Vortex formation in a free boundary layer according to stability theory *J. Fluid Mech.* **22** 371–83

J. Phys. D: Appl. Phys. **52** (2019) 354002

M Samimy *et al*

[4] Michalke A 1964 On the inviscid instability of the hyperbolic-tangent velocity profile *J. Fluid Mech.* **19** 543–56

[5] Crow S and Champagne F 1971 Orderly structure in jet turbulence *J. Fluid Mech.* **48** 547–91

[6] Brown G and Roshko A 1974 On density effects and large structure in turbulent mixing layers *J. Fluid Mech.* **64** 775–816

[7] Kibens V, Dorris J, Smith D and Mossman M 1999 Active flow control technology transition: the Boeing ACE Program *AIAA 30th Fluid Dynamics Conf., AIAA Paper 1999-3507* (https://doi.org/10.2514/6.1999-3507)

[8] Ho C-M and Huerre P 1984 Perturbed free shear layers *Annu. Rev. Fluid Mech.* **16** 365–424

[9] Samimy M, Webb N and Crawley M 2018 Excitation of free shear-layer instabilities for high-speed flow control *AIAA J.* **56** 1770–1

[10] Kendall J 1967 Supersonic boundary layer experiments *Proc. Boundary Layer Transition Study Group* vol 2 Aerospace Corporation Report TR-0158

[11] Martens S, Kinzie K and McLaughlin D 1994 Measurements of Kelvin–Helmholtz instabilities in a supersonic shear layer *AIAA J.* **32** 1633–9

[12] Corke T, Enloe C and Wilkinson S 2010 Dielectric barrier discharge plasma actuators for flow control *Ann. Rev. Fluid Mech.* **42** 505–29

[13] Samimy M, Kim J-H, Kastner J, Adamovich I and Utkin Y 2007 Active control of high-speed and high-Reynolds-number jets using plasma actuators *J. Fluid Mech.* **578** 305–30

[14] Utkin Y, Keshav S, Kim J-H, Kastner J, Adamovich I and Samimy M 2007 Development and use of localized arc filament plasma actuators for high-speed flow control *J. Phys. D: Appl. Phys.* **40** 685–94

[15] Little J 2019 Localized thermal perturbations for control of turbulent shear flows *AIAA J.* **57** 655–69

[16] Cattafesta L and Sheplak M 2011 Actuators for active flow control *Annu. Rev. Fluid Mech.* **43** 247–72

[17] Little J, Takashima K, Nishihara M, Adamovich I and Samimy M 2012 Separation control with nanosecond-pulse-driven dielectric barrier discharge plasma actuators *AIAA J.* **50** 350–65

[18] Macheret S, Shneider M and Miles R 2004 Magnetohydrodynamic and electrohydrodynamic control of hypersonic flows of weakly ionized plasmas *AIAA J.* **42** 1378–87

[19] Kelley C, Bowles P, Cooney J, He C, Corke T, Osborne B, Silkey J and Zehnle J 2014 Leading-edge separation control using alternating-current and nanosecond-pulse plasma actuators *AIAA J.* **52** 1–14

[20] Moreau E 2007 Airflow control by non-thermal plasma actuators *J. Phys. D: Appl. Phys.* **40** 605–36

[21] Kriegseis J, Duchmann A, Tropea C and Grundmann S 2013 On the classification of dielectric barrier discharge plasma actuators: a comprehensive performance evaluation study *J. Appl. Phys.* **114** 053301

[22] Leonov S, Bityurin V, Savelkin K and Yarantsev D 2002 Effect of electrical discharge on separation processes and shocks position in supersonic airflow *AIAA 40th Aerospace Sciences Meeting and Exhibit, AIAA Paper 2002-0355* (https://doi.org/10.2514/6.2002-355)

[23] Samimy M, Adamovich I, Webb B, Kastner J, Hileman J, Keshav S and Palm P 2004 Development and characterization of plasma actuators for high-speed jet control *Exp. Fluids* **37** 577–88

[24] Hahn C, Kearney-Fischer M and Samimy M 2011 On factors influencing arc filament plasma actuator performance in control of high speed jets *Exp. Fluids* **51** 1591–603

[25] Haack S, Cybyk B, Nedungadi A, Land H, Taylor T, Katz J, Ko H and Alvi F 2010 High-speed active flow control *Johns Hopkins APL Technical Digest* vol 28 pp 280–1

[26] Narayanaswamy V, Raja L and Clemens N 2012 Control of unsteadiness of a shock wave/turbulent boundary layer interaction by using a pulsed-plasma jet actuator *Phys. Fluids* **24** 1–23

[27] Bonnet J, Acher G, Audier P, Robert A, Lebedev A, Benard N and Moreau E 2017 Development and characterization of a pulsed jet actuator based on sonic flow controlled by plasma *10th Int. Symp. on Turbulence and Shear Flow Phenomena* p 3A-1

[28] Adelgren R G, Elliott G S, Crawford J B, Carter C D, Donbar J M and Grosjean D F 2005 Axisymmetric jet shear-layer excitation by laser energy and electric arc discharges *AIAA J.* **43** 776–91

[29] Samimy M, Kim J-H, Kearney-Fischer M and Sinha A 2010 Acoustic and flow fields of an excited high Reynolds number axisymmetric supersonic jet *J. Fluid Mech.* **656** 507–29

[30] Moore C 1977 The role of shear-layer instability waves in jet exhaust noise *J. Fluid Mech.* **80** 321–67

[31] Barone M and Lele S 2005 Receptivity of the compressible mixing layer *J. Fluid Mech.* **540** 301–35

[32] Adamovich I V, Leonov S B, Frederickson K, Zheng J, Cui Y and Khoo B C 2017 Thermal perturbations generated by near-surface electric discharges and mechanisms of their interaction with the airflow *55th AIAA Aerospace Sciences Meeting, AIAA Paper 2017-1339* (https://doi.org/10.2514/6.2017-1339)

[33] Gaitonde D and Samimy M 2011 Coherent structures in plasma-actuator controlled supersonic jets: axisymmetric and mixed azimuthal modes *Phys. Fluids* **23** 95–104

[34] Crawley M, Kuo C-W and Samimy M 2018 Vortex dynamics and sound emission in excited high-speed jets *J. Fluid Mech.* **839** 313–47

[35] Webb N, Clifford C and Samimy M 2013 Control of oblique shock wave/boundary layer interactions using plasma actuators *Exp. Fluids* **54** 1–13

[36] Yugulis K, Hansford S, Gregory J and Samimy M 2013 Control of high subsonic cavity flow using plasma actuators *AIAA J.* **52** 1542–54

[37] Webb N and Samimy M 2017 Control of supersonic cavity flow using plasma actuators *AIAA J.* **55** 3346–55

[38] Roupassov D, Nikipelov A, Nudnova M and Starikovskii A 2009 Flow separation control by plasma actuator with nanosecond pulsed-periodic discharge *AIAA J.* **47** 168–85

[39] Esfahani A, Webb N and Samimy M 2018 Stall cell formation over a post-stall airfoil–effects of active perturbations using plasma actuators *Exp. Fluids* **59** 132

[40] Singhal A, Castañeda D, Webb N and Samimy M 2018 Control of dynamic stall over a NACA 0015 airfoil using NS-DBD plasma actuators *AIAA J.* **56** 78–89

[41] Rethmel C, Little J, Takashima K, Sinha A, Adamovich I and Samimy M 2011 Flow separation control using nanosecond pulse driven DBD plasma actuators *Int. J. Flow Control* **3** 213–32

[42] Aleksandrov N L, Kindysheva S V, Nudnova M M and Starikovskiy A Y 2010 Mechanism of ultra-fast heating in a non-equilibrium weakly ionized air discharge plasma in high electric fields *J. Phys. D: Appl. Phys.* **43** 255201

[43] Leonov S B, Petrishchev V and Adamovich I V 2014 Dynamics of energy coupling and thermalization in barrier discharges over dielectric and weakly conducting surfaces on μs to ms time scales *J. Phys. D: Appl. Phys.* **47** 465201

[44] Zheng J G, Cui Y D, Zhao Z J, Li J and Khoo B C 2016 Investigation of airfoil leading edge separation control with nanosecond plasma actuator *Phys. Rev. Fluids* **1** 2016

[45] Esfahani A, Webb N and Samimy M 2019 Flow separation control over a thin post-stall airfoil: effects of excitation frequency *AIAA J.* **57** 1–13

J. Phys. D: Appl. Phys. **52** (2019) 354002

M Samimy *et al*

[46] Visbal M 2014 Numerical exploration of flow control for delay of dynamic stall on a pitching airfoil *32nd AIAA Applied Aerodynamics Conf., AIAA Paper 2014-2044* (https://doi.org/10.2514/6.2014-2044)

[47] Visbal M 2015 Control of dynamic stall on a pitching airfoil using high-frequency actuation *53rd AIAA Aerospace Sciences Meeting, AIAA Paper 2015-1267* (https://doi.org/10.2514/6.2015-1267)

[48] Visbal M and Benton S 2018 Exploration of high-frequency control of dynamic stall using large-Eddign simulations *AIAA J.* **56** 2974–91

[49] Crighton D and Gaster M 1976 Stability of slowly diverging jet flow *J. Fluid Mech.* **77** 397–413

[50] Michalke A 1984 Survey on jet instability theory *Prog. Aerosp. Sci.* **21** 159–99

[51] Ray P, Cheung L and Lele S 2009 On the growth and propagation of linear instability waves in compressible turbulent jets *Phys. Fluids* **21** 2009

[52] Gudmundsson K and Colonius T 2011 Instability wave models for the near-field fluctuations of turbulent jets *J. Fluid Mech.* **689** 97–128

[53] Garnaud X, Lesshafft L, Schmid P and Huerre P 2013 The preferred mode of incompressible jets: linear frequency response analysis *J. Fluid Mech.* **716** 189–202

[54] Hussain A and Zaman K 1981 The 'preferred mode' of the axisymmetric jet *J. Fluid Mech.* **110** 39–71

[55] Hileman J, Thurow B, Caraballo E and Samimy M 2005 Large-scale structure evolution and sound emission in high-speed jets: real-time visualization with simultaneous acoustic measurements *J. Fluid Mech.* **544** 277–307

[56] Adrian R, Christensen K and Liu Z-C 2000 Analysis and interpretation of instantaneous turbulent velocity fields *Exp. Fluids* **29** 275–90

[57] Hunt J, Wray A and Moin P 1988 Eddies, stream, and convergence zones in tubulent flows *Studying Turbulence Using Numerical Simulation Databases. II. Proc. 1988 Summer Program* p 193

[58] Samimy M, Kearney-Fischer M, Kim J-H and Sinha A 2012 High-speed and high-Reynolds-number jet control using localized arc filament plasma actuators *J. Propul. Power* **28** 269–80

[59] Kuo C-W, Cluts J and Samimy M 2017 Effects of excitation around jet preferred mode Strouhal number in high-speed jets *Exp. Fluids* **58** 1–12

[60] Kearney-Fischer M, Kim J-H and Samimy M 2011 Noise control of a high Reynolds number high speed heated jet using plasma actuators *Int. J. Aeroacoust.* **10** 635–58

[61] Kearney-Fischer M, Kim J-H and Samimy M 2011 A study of Mach wave radiation using active control *J. Fluid Mech.* **681** 261–92

[62] Lighthill M J and Newman M H A 1952 On sound generated aerodynamically I. General theory *Proc. R. Soc.* A **211** 564–87

[63] Kopiev V F *et al* 2014 Instability wave control in turbulent jet by plasma actuators *J. Phys. D: Appl. Phys.* **47** 505201

[64] Kopiev V F *et al* 2015 Instability wave control in turbulent jet by acoustical and plasma actuators *Prog. Flight Phys.* **7** 211–28

[65] Kuo C-W, Cluts J and Samimy M 2017 Exploring physics and control of twin supersonic circular jets *AIAA J.* **55** 68–85